Sortilin regulates blood-brain barrier integrity

Toth, Andrea E; Helms, Hans C; Harazin, Andras; Johnsen, Kasper B; Goldeman, Charlotte; Burkhart, Annette; Thomsen, Maj S; Kempen, Paul J; Klepe, Adrian; Lipka, Dora V; Møller, Peter L; Andresen, Thomas L; Nyegaard, Mette; Moos, Torben; Brodin, Birger; Nielsen, Morten S

Published in:
The FEBS Journal

DOI (link to publication from Publisher):
10.1111/febs.16225

Publication date:
2022

Document Version
Accepted author manuscript, peer reviewed version

Sortilin regulates blood-brain barrier integrity

Andrea E. Toth[1,2], Hans C. Helms[2,3], Andras Harazin[1], Kasper B. Johnsen[2,5], Charlotte Goldeman[2,3], Annette Burkhart[2,4], Maj S. Thomsen[2,4], Paul J. Kempen[2,5], Adrian Klepe[1], Dora V. Lipka[1], Peter L. Møller[1], Thomas L. Andresen[2,5], Mette Nyegaard[1], Torben Moos[2,4], Birger Brodin[2,3], Morten S. Nielsen[1,2]

[1]Department of Biomedicine, Faculty of Health, Aarhus University, Høegh-Guldbergsgade 10, 8000 Aarhus, Denmark;

[2]Lundbeck Foundation Research Initiative on Brain Barriers and Drug Delivery;

[3]Department of Pharmacy, Faculty of Health and Medical Sciences, University of Copenhagen, Universitetsparken 2, 2100 Copenhagen, Denmark

[4]Laboratory of Neurobiology, Biomedicine Group, Department of Health Science and Technology, Aalborg University, Fr. Bajers Vej 3B, 1.216, 9220 Aalborg East, Denmark

[5]Section for Biotherapeutic Engineering and Drug Targeting, Department of Health Technology, Technical University of Denmark, 2800 Kgs. Lyngby, Denmark

§Corresponding author: Morten S. Nielsen, Department of Biomedicine, Høegh-Guldbergsgade 10, 8000 Aarhus, Denmark, tel. +45 28992387, e-mail: mn@biomed.au.dk.

Running title: Sortilin, a new player at the blood-brain barrier

Abbreviations:

AJ, adherent junction; BBB, blood-brain barrier; BCH, 2-aminobicyclo[2.2.1]heptane-2-carboxylic acid; BEC, brain endothelial cell; BSA, bovine serum albumin; cAMP, 8-(4-chlorophenylthio) adenosine-3´,5´-cyclic monophosphate; DAB, 3,3′-diaminobenzidine tetrahydrochloride; DMEM, Dulbecco's modified Eagle medium; ERK, extracellular signal-regulated kinases; GAPDH, glyceraldehyde 3-phosphate dehydrogenase; GFAP, glial fibrillary acidic protein; GLUT1/SLC2A1, glucose transporter 1; HBSS, Hank's balanced salt solution; HRP, horseradish peroxidase; ICP-MS, inductively coupled plasma mass spectrometry; KO, knock-out mutant; KPBS, potassium phosphate-buffered saline; LAT1/SLC7A5, large neutral

This article has been accepted for publication and undergone full peer review but has not been through the copyediting, typesetting, pagination and proofreading process, which may lead to differences between this version and the Version of Record. Please cite this article as doi: 10.1111/febs.16225

amino acid transporter; M6PR, mannose 6-phosphate receptor; MAPK, mitogen-activated protein kinases; MDR1/ABCB1, multidrug resistance mutation 1; MTT, 3-(4,5-dimetylthiazol-2-yl)-2,5-diphenyltetrazolium bromide; NG2, neuron-glial antigen 2; P_{app}, apparent permeability coefficient; PBS, phosphate-buffered saline; PDS, plasma derived serum; PI3K, phosphatidylinositol 3-kinase; RT-qPCR, real-time quantitative PCR; Sort1, sortilin; TEER, transendothelial electrical resistance; TEM, transmission electronmicroscopy; TJ, tight junction; VE-cadherin, vascular endothelial cadherin; Vps10, vacuolar protein sorting 10 protein; WT, wild type; ZO-1, zonula occludens-1

Keywords: adherent junction / blood-brain barrier / brain endothelial cells / sortilin / tight junction

Conflict of interest

The authors declare no conflict of interest.

Data accessibility statement

This study includes no data deposited in external repositories.

Abstract

Brain homeostasis depends on the existence of the blood-brain barrier (BBB). Despite decades of research, the factors and signalling pathways for modulating and maintaining BBB integrity are not fully elucidated. Here, we characterize the expression and function of the multifunctional receptor, sortilin, in the cells of the BBB, *in vivo* and *in vitro*. We show that sortilin acts as an important regulatory protein of the BBB's tightness. In rats lacking sortilin, the BBB was leaky, which correlated well with relocated distribution of the localisation of zonula occludens-1, VE-cadherin and β-catenin junctional proteins. Furthermore, the absence of sortilin in brain endothelial cells resulted in decreased phosphorylation of Akt signalling protein and increased the level of phospho-ERK1/2. As a putative result of MAPK/ERK pathways activity, the junctions between the brain endothelial cells were disintegrated and the integrity of the BBB became compromised. The identified barrier differences between wild type and *Sort1-/-* brain endothelial cells can pave the way for a better understanding of sortilin's role in the healthy and diseased BBB.

1. Introduction

The capillaries of the brain constitute a highly specialised structure, the so-called blood-brain barrier (BBB). The physiological barrier element of the BBB is the specialised endothelium formed by brain endothelial cells (BECs). To acquire and maintain the specific barrier attributes, BECs need the support of their neighbouring cells, which mainly are astrocytes and pericytes. The tight and healthy BBB protects the brain from exogenous and endogenous compounds with neurotoxic properties and strictly controls the exchange of solutes between the blood and the central nervous system [1]. To fulfil these functions, receptors, transporters, and efflux pumps are localised in the membranes of BECs in a function-specific manner [2]. For instance, the majority of the P-glycoprotein efflux pumps (MDR1/ABCB1) are located at the luminal membrane of BECs where they limit the brain penetration of lipophilic xenobiotics and drugs from the blood [3]. On the other hand, to supply the brain with the necessary nutrients, certain transporters need to be present nearly equally at both surfaces of the BECs such as the glucose transporter 1 (GLUT1/SLC2A1) [4] and the large neutral amino acid transporter (LAT1/SLC7A5) [5]. Brain interstitial spinal fluid homeostasis depends on the integrity of the barrier therefore BECs are connected laterally by numerous tight (TJs) and adherent junction complexes (AJs). These complexes are built up from highly specialised transmembrane receptors, such as claudins, and cadherin family proteins and their cytoplasmatic linker proteins e.g., zonula occludens proteins, and the catenins [6]. Claudin-5 is the major constitutive claudin among the TJs of the BBB [7], while in the AJs the vascular endothelial cadherin (VE-cadherin) is the dominant transmembrane protein [8]. Both transmembrane proteins are anchored intracellularly to the actin cytoskeleton via direct or indirect interaction with the zonula occludens-1 (ZO-1) protein [9, 10]. Among the catenins, β-catenin has received increased attention due to its dual role as a cytoplasmic anchor-protein for VE-cadherin and as a central element of the Wnt/β-catenin signalling pathway [11]. Besides the Wnt/β-catenin pathway, several other signalling pathways have an important function in the regulation of the integrity of the BBB including the phosphatidylinositol 3-kinase (PI3K)/Akt and the mitogen-activated protein kinase/extracellular signal-regulated protein kinase (MAPK/ERK) pathways. [12]. Especially, altered MAPK signalling pathway has been reported in

several diseases to cause BBB disruption [13]. Despite several years of research, there remained gaps in our knowledge of how and which proteins influence the BBB under normal and pathophysiological conditions.

In recent years, sortilin has received a great deal of attention due to its fundamental role in health and diseases [14]. Sortilin is a member of the vacuolar protein sorting 10 protein (Vps10) domain family and is located mainly perinuclear in the late Golgi apparatus and endosomes [15]. Sortilin binds to various cargo proteins and regulates their surface localisation, secretion or degradation in lysosomes. However, 10% of sortilin is found on the cell membrane where it functions as an endocytic receptor with high capacity. After endocytosis the internalized ligand-receptor complex is transferred to the endo-lysosomal system for retrograde transport to the trans-Golgi network or for lysosomal degradation [16]. Sortilin-mediated vesicle trafficking affects the cellular levels and activities of numerous substrate proteins such as signalling receptors, enzymes, and growth factors. Therefore, sortilin is characterized as a multifunctional receptor [14]. Physiologically, sortilin plays a key role in various important functions, ranging from normal biological processes such as neuronal survival [17], and glucose metabolism [18] to the influence of pathological processes underlying neurodegenerative diseases [19]. Moreover, it has been shown to have a pivotal role in cardiovascular and metabolic disorders [20, 21]. Sortilin is abundantly expressed in several tissues and organs especially in the brain [15]. Therefore, it has mainly been investigated in neurons and to some extent in glial cells [22]. However the role of sortilin in the cells of the BBB has previously not been addressed except from expression data in large gene sequencing databases [23-25] (Data ref: [26, 27]).

The aim of the present work was to investigate the expression of sortilin in the brain microvessels, and the other cells of the BBB, including BECs, astrocytes and pericytes, and to elucidate the role of sortilin in maintaining the integrity of the BBB. We primarily focus on sortilin's expression in the BECs which are the cells that forms the physical basis of the BBB. The applied *in vivo* and *in vitro* approaches describe specific cell and organ functions in wild-type (WT-) and *Sort1-/-* knock-out (KO) animals and thereof isolated primary cells. Since sortilin is known to be involved in the pAkt signalling pathway we also evaluate the phosphorylation of Akt and ERK1/2 in our models.

2. Results

2.1 Sortilin is expressed in the cells of the brain microvessels

To study what role sortilin plays at the BBB, we first investigated the expression of *Sort1* gene in the cell types constituting brain microvessels. We found that the *Sort1* gene is highly expressed in BECs, as well as in astrocytes and pericytes from wildtype rats [**Fig 1A**]. To further validate *Sort1* genes expression, Western blot was performed on isolated microvessels, BECs, astrocytes, and pericytes. The BECs and astrocytes were grown in Transwell setup as non-contact co-culture [28] and pericytes as monoculture [29]. In agreement with the gene expression data, sortilin was detectible in a considerable amount in the lysate of WT-microvessels, -BECs, -astrocytes, and -pericytes [**Fig 1B**]. Previously study has validated the lack of sortilin expression in *Sort1-/-* rats, and accordingly sortilin was not present in the lysate of microvessels, BECs, astrocytes and pericytes from KO rats [**Fig 1B**] [30]. The subcellular localisation of sortilin was further characterised by immunocytochemistry [**Fig 1C-F**]. The majority of sortilin was localised around the nucleus in the WT-BECs, -astrocytes and -pericytes [**Fig 1D-G**], and a co-staining with cation independent mannose 6-phosphate receptor suggests the majority of sortilin is perinuclear located in the trans-Golgi network [**Fig 1C**]. Consistent with the Western blot data, we observed positive staining for sortilin only in the WT cells and not in the cells of the sortilin knock-out rats. The BECs had the typical elongated morphology and formed confluent layers. Immunocytochemistry staining of the tight junction protein claudin-5 delineated the endothelial cell borders [**Fig 1E**]. The cell–cell attachment was continuous in both groups, as judged by the claudin-5 staining. Astroglia's expressing glial fibrillary acidic protein (GFAP) showed a multipolar shape with long processes. This stellate shape could be observed in the WT- as well as in the KO-cells [**Fig 1F**]. Pericytes were characterized by their large cell size, polygonal cell shape, branched morphology, and positive staining for neuron-glial antigen 2 (NG-2) [**Fig 1G**].

2.2 Sortilin-KO brain microvessels displays a decreased integrity

Having established that sortilin was indeed expressed in brain microvessels, we focused on the role of sortilin in BBB integrity, using the compounds oxaliplatin and investigating endogenous albumin leakage. Oxaliplatin is a low molecular weight (397 Da) BBB-impermeable chemotherapeutic drug previously used for the investigation of paracellular leakage [31]. Oxaliplatin was injected in the tail vein of WT- and KO-rats. Cortical brain microvessels of the KO-rats had reduced integrity, as evidence by a 50 % increase in the accumulation of oxaliplatin

(26.15 ± 2.82 ng/g) in KO-brain homogenates compared to the WT controls (17.01 ± 2.25 ng/g) [**Fig 2A**].

In addition to the paracellular tightness, we examined the transcellular permeability of the capillaries by looking for albumin leakage. Albumin occurs naturally in the blood and is transported only in low amount across the endothelium of intact microvessels [32]. The top panel in **Fig 2B** shows representative images of the cortex where there is no albumin immunoreaction in either WT- or the KO-cortex, indicating normal vesicular paracellular transport in absence of the sortilin as well. The bottom panel demonstrates representative images of the choroid plexus as positive controls. The choroid plexus has positive albumin labelling in both groups, which indicates that the immunolabelling is working [**Fig 2B**]. Additionally, the ultrastructural of 50 brain capillaries were analysed by transmission electronmicroscopy (TEM) [**Fig 2C**]. TEM images did not any show significant differences in the endothelial wall thickness between the WT- (226 ± 19 nm) and KO-cortex (226 ± 17 nm), indicating no ongoing endothelial inflammation that could contribute to vessel leakiness [**Fig 2C-D**]. The data indicates that the sortilin KO cells have less tight barrier that allows more influx of small molecules by paracellular transport, whereas transcellular vesicular transport is not affected.

2.3 Sortilin is involved in maintaining BBB integrity

To investigate the functionality of the BECs, we co-cultured brain capillary endothelial monolayers with astrocytes, also known as no-contact co-culture BBB model. As illustrated by **Fig 3A**, WT-BECs were co-cultured with WT-astrocytes and similarly, KO-BECs were co-cultured with KO-astrocytes. We examined the tightness of the *in vitro* BBB models [**Fig 3B-C**] and the function of selected influx and efflux transporters using their radiolabelled substrates [**Fig 3D-F**].

In parallel with the *in vivo* data, the KO-BBB model was leaky for the paracellular permeability marker, sodium-fluorescein *in vitro*. The KO-BECs showed doubled permeability values ($5.74 \times 10^{-6} \pm 1.27 \times 10^{-6}$ cm/s) compared to WT-BECs ($2.72 \times 10^{-6} \pm 0.51 \times 10^{-6}$ cm/s) [**Fig 3B**]. Accordingly, the TEER values of the KO-endothelial monolayer (293 ± 39 Ω x cm^2) were nearly two times lower, than for the WT-endothelial monolayer (553 ± 18 Ω x cm^2). While WT-BECs co-cultured with KO-astrocytes did not show significantly higher TEER [**Fig 3C**]. The TEER values indicate the tightness of the confluent BECs' layers and reflect the permeability of the intercellular junctions for sodium ions [33].

The BECs are polarised cells with the apical membrane facing the blood and the abluminal membrane at the brain side. The polarity of the cells arise from the differential expression of specific transporters in the luminal and abluminal membranes [3]. To analyse the functional polarity in BEC's from WT and KO rats, the efflux transporter activity of P-glycoprotein was investigated in a bidirectional transport study [**Fig 3D**]. Luminal-to-abluminal (A-B) and abluminal-to-luminal (B-A) transendothelial fluxes of the P-glycoprotein substrate, ^{3}H-digoxin was measured. The WT-BECs displayed steady-state permeability values of $2.53 \pm 0.07 \times 10^{-6}$ cm/s (A-B) and $5.72 \pm 0.08 \times 10^{-6}$ cm/s (B-A). Similarly, the KO-BECs exhibited permeability values of $2.53 \pm 0.27 \times 10^{-6}$ cm/s (A-B) and $5.64 \pm 0.06 \times 10^{-6}$ cm/s (B-A). In both BBB-models, the flux from the abluminal to the luminal compartment (B-A) was more than two-fold higher than the flux in the opposite direction. Therefore, the net efflux ratio (P_{B-A}/P_{A-B}) was nearly 2.2 indicating active efflux transport. In both cases, the specific P-glycoprotein inhibitor, zosuquidar inhibited the polarized efflux [**Fig 3D**]. Thus, both models retain functional P-glycoprotein expression. These demonstrate functionally active and polarized efflux transport by P-glycoprotein with no difference between the WT- and the KO-BBB models. Furthermore, the uptake of ^{3}H-glucose by the GLUT1 was very low (approximately 0.008% of the added tracer) in both BBB models and was not affected by adding unlabelled glucose for competition [**Fig 3E**]. The LAT1 facilitated transport of ^{3}H-L-leucine in the presence or absence of the specific LAT-1 inhibitor 2-aminobicyclo[2.2.1]heptane-2-carboxylic acid (BCH), was investigated as well. The transport of ^{3}H-L-leucine was inhibited approximately 40-45% by BCH which indicated functional LAT1 transporter in both models. Although there was a difference between the leucine uptake of the WT- and the KO-BECs, it did not reach statistical significance [**Fig 3F**].

2.4 Sortilin influences the junctional proteins of the BECs

Altered TEER and permeability values [**Fig 3B-C**] can indicate changes in the structure and the expression of the inter-endothelial junctions [34]. Therefore, we have investigated the protein level and the localisation of the most well-characterized TJ and AJ proteins namely ZO-1, claudin-5, β-catenin, and VE-cadherin [**Fig 4**]. To quantify the observed differences in localisation, the fluorescence intensity of the junctional proteins at the cell border and in the cytoplasm were measured, and the ratio of these values (localisation ratio) were compared between the WT-BECs and KO-BECs [**Fig 4**].

The ZO-1 TJ protein showed a lower localisation ratio in the KO-BECs than in the WT-BECs [**Fig 4A**]. Accordingly, less fluorescence intensity was measured at the cell border of the KO-BECs. However, no difference was detectable in the protein amount of ZO-1 between the two groups [**Fig 4B**], indicating changes only in the localisation of this tight junction protein. In the case of claudin-5, no significant difference was seen neither in terms of localisation [**Fig 4C**], nor in western blot [**Fig 4D**]. Similarly to ZO-1, the other cytoplasmic junctional protein β-catenin resulted in a lower localisation ratio in the KO-BECs and β-catenin staining could be seen around the nuclei in the KO-BECs [**Fig 4E**]. The protein level of β-catenin in KO-BECs was markedly decreased (78.87 ± 6.12%) compared to the WT-BECs [**Fig 4F**]. Since β-catenin expression was changed, we have investigated its transmembrane linking partner, VE-cadherin [**Fig 4G-H**]. A lower localisation ratio in the KO-BECs was observed and more proteins were visible in the cytoplasm of these cells [**Fig 4G**]. However, the protein amount of VE-cadherin did not differ between the WT- and the KO-group [**Fig 4H**]. Images quantification using high content line scan of capillaries is not possible with our methods, wherefore no in vivo data has been acquired. Overall, the results indicated that the observed BBB leakage [**Fig 2A, Fig 3B-C**] is caused by re-localisation of the junctional proteins.

2.5 Sortilin and the signalling pathways in BECs

To explore the mechanisms of how sortilin influences the localisation of junctional proteins, we examined the activation of those key signalling pathway proteins, which are associated with both sortilin and the junctional proteins.

The absence of sortilin significantly decreased the phosphorylation of Akt protein (pAkt; 59.17 ± 7.04%) in the KO-BECs [**Fig 5A**]. There was no statistically significant difference in the amount of total-Akt protein between the KO- and the WT-BECs. Still, the level of total-Akt was slightly lower in KO-BECs (79.37 ± 6.15%), which was likely caused by the difference in phospho-Akt. This indicated that there was no difference in the level of un-phosphorylated Akt between the two genotypes. Accordingly, the ratio of phospho-Akt to total-Akt (pAkt/T-Akt) was significantly lower in the KO-group (KO: 0.97 ± 0.10; WT: 1.39 ± 0.13).Since there is less phospho-Akt in the KO-BECs to inhibit the activation of the MAPK pathway, the phosphorylation of ERK1/2 was increased by the same extent (pERK1/2; 146 ± 6 %) in those cells [**Fig 5B**]. This resulted in a significant difference in the level of total-ERK1/2 (KO: 3 ± 7.0 %) and in the pERK1/2/T-ERK1/2 (KO: 0.66 ± 0.06; WT: 0.87 ± 0.06). Finally, we added a phospho-Akt

inhibitor which evaluated by western blot resulted in an almost complete blocking of Akt phosphorylation. Analysing the wildtype BEC in this set-up displayed a drop in TEER values, but re-localisation of β-catenin and VE-cadherin as observed in the Sortilin KO was not significant [**Fig 5C,** β-catenin not shown]. Attempt to increase the amount of phospho-Akt via stimulation of sortilin using sortilin ligand Spadin failed [**Fig 5C**] [35].

These results suggested that sortilin maintained the phosphorylation level of Akt protein in WT-BECs resulting in inhibited activation of the MAPK/ERK1/2 pathway. In the absence of sortilin, the amount of phospho-Akt protein decreased, while the pERK to ERK ration was increased. This could indicate a general activation in the MAPK pathway which might be related to the changed localisation of junctional proteins and the tightness of the BEC monolayer. As the MAPK/ERK is known to influence the proliferation and migration of other endothelial cells, we did test the viability and proliferation of the sortilin KO BEC in relation to wildtype BEC using a MTT proliferation kit. We did now observe any changes (WT BEC 97.92 ± 3.18; KO BEC 100.0 ± 1.84; p=0.576), however the other downstream effect of the kinase pathway should be further analysed in the future.

3. Discussion

Sortilin has fundamental biological functions in different organs and tissues of the body and has been intensively analysed over the last decade [19]. Since sortilin is abundantly expressed in the brain [15, 36], its role in neurons and to some extent in certain glia cells of different brain regions have been investigated [22]. However, the brain microvessels including the cells of the BBB have been neglected. Here, we provided the first evidence on the presence of sortilin in the cells of the BBB. We use a BBB model based on primary rat cells as these has been validated to mimic the in vivo barrier with respect to tightness, transporter activity and receptors [37]. We have shown that sortilin is expressed and is detectable at a considerable protein level in BECs as well as in other cells of the BBB, such as astrocytes and pericytes. We have also shown that sortilin has a perinuclear localization in these cells. These findings agree with other studies in different cell types describing the perinuclear localisation of sortilin in transcellular vesicles and the trans-Golgi network [16]. Moreover, previous wide-range gene expression studies support our findings which have reported *Sort1* gene to be expressed in BECs, astrocytes, and pericytes from both mouse and

human origin ([23-25] (Data ref: [26, 27]). Only a few studies mention the role of sortilin in peripheral endothelial cells, but sortilin has been found to be involved in myocardial hypoxia/reoxygenation injury [38] and in activation of membrane NADPH oxidase [39]. However, the focus of these studies was not primarily to describe the role of sortilin in endothelial cells. The data presented here provide the framework for future studies to explore the function and importance of sortilin in other endothelial cells. We have focused on the role of sortilin in BECs of the microvessels since these cells serve as the anatomical basis and forms the main barrier of the BBB. Since the Vps10p-D receptors are known to bind and sort several growth factors, the effect on BBB integrity of sortilin expression in astrocytes would be important to study [19, 40]. Less is known about Vps10p-D receptors in pericytes, but SorCS-2 is upregulated in mice pericytes during ischemia-reperfusion injury and might have a function in signalling in inflammation of pericytes [41]. The role of sortilin in other cells of the BBB such as astrocytes and pericytes would therefore be important to explore in future studies.

Sortilin is primarily a sorting receptor, which mediates the vesicular trafficking of various substrate proteins involved in physiological and pathological processes [42]. For instance in striated muscle, sortilin transfers the insulin-regulated glucose transporter 4 from the storage vesicles to the plasma membrane, thus accelerating the uptake of glucose and inhibiting the progression of diabetes [43]. Therefore, we have investigated the glucose uptake in BECs. The BECs of the BBB express a different type of glucose transporter, the so-called insulin-independent GLUT1 [44]. This glucose transporter was not affected by the lack of sortilin in our experiments. In addition, the amino acid transporter LAT1 has proved to function independently from the presence of sortilin. The BECs are polarised cells and for maintenance of the polarity and proper function of these cells, correct sorting of proteins is essential [2]. One of the most important efflux pumps of the BECs, the P-glycoprotein, is located at the luminal membrane where it limits the brain penetration of lipophilic xenobiotics and drugs from the blood [3]. Therefore, we have investigated the efflux transporter activity of P-glycoprotein by a bidirectional transport study. However the absence of sortilin did not change the function and the polarized activity of P-glycoprotein. This indicates that the sortilin receptor is not crucial for the polarisation of BECs, but future studies are needed to determine whether sortilin is a sorting receptor for other essential transporters in the BECs.

Brain homeostasis depends on the integrity of the BBB. Therefore, we have further analysed the permeability and the tightness of the BBB both *in vivo* and *in vitro*. The microvessels and the

BECs of the KO-rats lacking sortilin were leaky to paracellularly transported oxaliplatin. Accordingly, the *in vitro* KO-BBB model has proved to be less tight than the WT. The increased permeability of sodium-fluorescein and the low transendothelial electrical resistance (TEER) values of the KO-BBB model pointed out that sortilin plays an important role in the integrity of the BBB. A leaky BBB is a common hallmark in pathological conditions such as Alzheimer's disease [45], hypercholesterolemia [46], and diabetes [46, 47]. Interestingly the dysfunction or downregulation of sortilin has been also connected to the progression of these diseases [48-50].

Under pathological conditions, the expression, posttranslational modification, trafficking, and localisation of junctional proteins change. In the healthy BECs, the majority of the junctional proteins are localised at the cell border giving strong fluorescent staining where the cells attach to each other. Only a low amount of proteins can be found in the cytoplasm [6, 34]. In KO-BECs, the junctional proteins showed an altered localisation profile compared to the ones in the WT-BECs. The intensity of ZO-1 has dropped at the cell border and more VE-cadherin and β-catenin adherent junctional proteins were visible in the cytoplasm. Additionally, the protein level of β-catenin was lower in these cells. To reveal the mechanisms of how sortilin influences the localisation of junctional proteins, we examined the activation of the key signalling pathway proteins, which are associated with both sortilin and the junctional proteins. Sortilin is known to induce the phosphorylation of Akt protein [51] and without an active PI3K/Akt pathway the protein level of sortilin dropped in insulin-resistant mice [52] and adipocytes [53]. These findings/observations were in agreement with the protein amount of pAkt fell dramatically in the KO-BECs compared to the WT-BECs in our experiments. Akt is a central protein, which communicates with several other signalling pathways [54]. Among these interactions, crosstalk between the PI3K/Akt and the MAPK/ERK pathways has been reported on multiple levels [55]. The phosphorylation of Raf protein by Akt abrogate Raf activity on MEK1/2 (mitogen-activated protein kinase kinase 1 and 2) and subsequently prevent the phosphorylation of ERK1/2 proteins in the MAPK/ERK pathway [56]. In line with these observations, ERK1/2 phosphorylation was highly increased in the KO-BECs. Increased phosphorylation of ERK1/2 and decreased level of sortilin were also described also in hepatic cells of obese and diabetic rats [50]. The MAPK/ERK signalling pathway is able to modulate paracellular transport by altering the molecular composition within TJ complexes [13]. In our study, an increased amount of pERK1/2 has been detected in KO-BECs and less ZO-1 was be found in the TJs. Accordingly to our findings, several papers have reported the absence or complete disappearance of ZO-1 from the cell border parallel with ERK1/2 activation [57-61].

Besides the ZO-1 protein, we have found disturbed localisation of VE-cadherin and β-catenin AJ proteins. Both of these proteins are anchored intracellularly to the actin cytoskeleton via indirect interaction with the ZO-1 protein [10]. Other studies have also found delocalisation of VE-cadherin and β-catenin from the cell border along with increased MAPK/ERK signalling pathway activity [62-64]. Our data does not fully elucidate the pathway by which sortilin affect the tightness of BEC, as a sudden inhibition of Akt phosphorylation only result in a slight but significant increase in permeability values, but not in relocation tight junction proteins. Either the relocation is a relatively gradual and cannot be observed within the timeframe of the experiment or more likely there are other mechanisms involved. This should be further investigated.

Collectively, our data suggested that sortilin is involved in maintenance the tightness of the BEC and thereby the integrity of BBB. The details of mechanism behind our observation are not fully clear, but in the absence of sortilin, the amount of pAkt drops and the MAPK/ERK pathway becomes activated. We suggest this changed activity of MAPK/ERK pathway in sortilin KO might affect the junctions of BECs which compromise the integrity of the BBB.

4. Materials and methods

4.1 Materials

All chemicals and reagents were purchased from Sigma-Aldrich (Missouri, USA) unless otherwise indicated.

4.2 Animals

Wild-type (WT) Sprague Dawley rats were obtained from Janvier labs, while *Sort1-/-* Sprague Dawley rats (KO) were purchased from Horizon Discovery and custom made, respectively, for breeding at the Animal Facility at Aarhus University. *Sort1-/-* is a 5 basepair deletion in exon 9 resulting in a stop codon, with subsequent complete destruction of the Vps10p-domain folding [30]. No mRNA splice variants or protein fragments were detected by sequencing or Western blot analysis. KO-animals were housed at the Animal Facility at Aarhus University in standard cages (Scanbur) in a temperature-controlled environment with a 12h light/12h dark cycle, light during daytime in a pathogen-free environment. Cages were cleaned every week and supplied with bedding and nesting material, a wooden stick, and a tunnel. Chow (Altromin 1324, Brogaarden, Denmark) and water were provided ad libitum. Animals were handled according to the Danish and European animal experimentation legislation (directive 2010/63/EU). All animal experiments were approved by the Danish Animal Experiments Inspectorate under the permission number 2017-15-0201-01192.

4.3 *In vivo* permeability experiment

The experiments were performed on 20 WT (~115 g) and 18 KO (~55 g) 3-weeks-old rats. Oxaliplatin was injected into the tail vein and left to circulate for 4 hours. Two animals per group were injected with saline water and used as blank. After 4 hours, animals were deeply anesthetized with Hypnorm/Dormicum (fentanyl/fluanisone mixed with midazolam and sterile water in a ratio of 1:1:2) and perfused in. The brain was extracted and cut into two halves. Each half was weighed and homogenized in a dunce homogenizer in 3.5 ml phosphate buffered saline (PBS) and snap frozen on dry ice, except the brains used for immunostaining. The oxaliplatin (MW: 397 Da) content was measured by inductively-coupled plasma-mass spectrometry (ICP-MS). The oxaliplatin content of the brain homogenate was plotted as a/the percentage of administrated dose as depicted from the sample taken immediately after administration and compared to the WT.

4.4 Primary cortical microvessels and cell culture isolations

Primary cortical microvessels were isolated from 3-week-old rats. The forebrains were collected in ice-cold sterile PBS. The meninges were removed and the grey matter was minced by scalpels into 1 mm^3 pieces.

For immunostaining of microvessels, the isolated grey matter was transferred to a grinder tube of a hand-held tissue homogenizer in Dulbecco's modified Eagle medium (DMEM). The microvessels were separated by centrifugation in 20% bovine serum albumin (BSA)-DMEM (1000×g, 20 min) from myelin containing elements. Next, the homogenate was filtered using 100 μm than 20 μm filter-mesh to isolate the intact microvessels. The brain capillaries were frozen in 10% DMSO-FBS mixture and frozen until further use. For visualisation in immunohistochemistry, microvessels were identified by claudin-5 immunopositivity.

For BEC and pericyte culturing, the tissue was digested with 1 mg/ml collagenase CLS2 (Worthington, USA) in DMEM for 1.5 hours at 37°C. The microvessels were separated by centrifugation in 20% BSA-DMEM (1000×g, 20 min) from myelin containing elements. The microvessels were further digested with 1 mg/ml collagenase-dispase (Roche) in DMEM for 1 hour. Microvascular BECs and pericytes clusters were separated on a 33% continuous Percoll gradient (1000×g, 10 min) and collected. The brain capillaries were frozen in 10% DMSO-FBS mixture and frozen until further use. BECs were cultured 1.5 weeks before the experiments as described in details below in the '*In vitro* BBB model constraction' section [**Fig 1C**].

Pure cultures of rat cerebral pericytes were obtained by prolonged, 2-week culture of isolated rat brain microvessels fragments that contain pericytes beside endothelial cells. Pericytes' survival and proliferation were favoured by selective culture conditions, using uncoated dishes, and DMEM supplemented with 10% FBS and antibiotics as described in a previous paper [65]. The culture medium was changed every twice a week. Cultured brain microvascular pericytes show typical morphology of large, flat multipolar cells with several branches in accordance with literature data [65]. Pericyte cultures were regularly checked for NG2 positivity which is a well-known marker for pericytes [**Fig 1F**].

Isolation of rat astrocytes was performed according to a previously described method [28]. Briefly, cultures of glial cells were prepared from newborn rats (1-2 days old). After removal of the meninges, the cortical pieces of the brain were mechanically dissociated, plated in poly-L-lysine coated T75 flasks (Thermo Fisher Scientific, Roskilde, Denmark), and kept for minimum of

3 weeks in DMEM containing 1% penicillin/streptomycin, and 10% FBS before being frozen. Minimum two weeks before co-culture, astrocytes were thawed and grown as above described in 12-well plate. Once the astrocytes reached 100% confluence, the medium was changed every three days. In confluent glia cultures, at least 90% of cells were immunopositive for GFAP [**Fig 1E**].

4.5 *In vitro* BBB model

All cell cultures were maintained in a humidified incubator with 5% CO_2 at 37°C. For primary cultures of cerebral endothelial cells, the rat brain capillaries were plated in T75 flasks coated with collagen IV (100 μg/ml) and fibronectin (100 μg/ml) in DMEM/F12 medium supplemented with 10% plasma-derived bovine serum (PDS; First Link Ltd, Wolverhampton, UK), basic fibroblast growth factor (1 ng/ml), heparin (15U), insulin-transferrin-selenium and gentamicin (5 μg/ml). Puromycin (4 μg/ml) was added to the medium for the first 3 days to obtain a pure culture of BECs and remove contaminating cells. Cells were grown until 70% confluency then passaged onto 1.12 cm^2 polycarbonate Transwell® filter inserts with 0.4 μm pore size (Costar, Corning, Kennebunk, ME, USA) at a density of 1-2 × 10^5 cells/cm^2. From the following day after seeding them on inserts, BECs were kept in a non-contact co-culture with rat astrocytes on the bottom of the 12-well culture dish. When the BECs had reached confluence, approximately 2 days after co-culture media on BECs and astrocytes have been changed and were supplied with differentiation factors: 550 nM hydrocortisone, 250 μM 8-(4-chlorophenylthio)adenosine-3′,5′-cyclic monophosphate (cAMP) and 17.5 μM RO-201724. Sample collection was carried out on the next day. The tightness of the *in vitro* BBB models was monitored by measuring transendothelial electrical resistance (TEER).

Two different models were used in this study [**Fig 3A**]; namely, the WT-BBB model and the KO-BBB model. For the WT model, we co-cultured WT-BECs with WT-astrocytes. To create the KO-BBB model, KO-BEC were co-cultured with KO-astrocytes at the same time and the same way as the WT.

Inhibiting the phosphorylation of Akt protein, Akti-1/2 (R&D Systems, Minneapolis, MN, USA) was used in 10 μM concentration for 1 hour at 37°C. Inhibiting sortilin, spadin (part of sortilin propeptide) was used in 100 nM concentration for 1 hour at 37°C. Control groups received only culture medium.

4.6 Measurement of tightness and permeability *in vitro*

TEER value reflects the tightness and the permeability of intercellular junctions for ions. TEER was measured by an EVOM resistance meter using EndOhm-12 cup system (World Precision Instruments Inc., Sarasota, FL, USA) and expressed relative to the surface area ($\Omega \times cm^2$). TEER values of cell-free inserts were subtracted from the measured data and presented as percent of the WT group.

To measure the permeability across endothelial cell layers, a small molecular weight (MW) marker sodium fluorescein (MW: 376 Da) was used. The molecular weight of the *in vitro* used permeability marker is comparable to the *in vivo* used oxaliplatin (MW: 397 Da). Cells were seeded onto Transwell inserts and grown as described above. Inserts with confluent layers were transferred to 12-well plates containing 1.5 mL DMEM phenol red-free medium (Gibco, Life technologies), which was the abluminal (lower) compartment in the permeability experiments. In the upper chambers (luminal compartment), the culture medium was replaced by 500 mL of DMEM phenol red-free medium containing 10 µg/mL sodium fluorescein and 1% BSA. The plates were kept in a 37°C incubator with 5% CO_2 on a horizontal shaker (150 rpm). To minimise luminal to abluminal transport, inserts were transferred at 20, 40, and 60 min to a new well containing DMEM phenol red-free medium. After 1-hour incubation, concentrations of the marker molecules in samples from the abluminal (lower) compartments were determined by Enspire multimode plate reader (PerkinElmer Inc, Lillestrøm, Norway). Sodium fluorescein concentration was measured by fluorescent spectrophotometry (emission: 525 nm, excitation: 440 nm). Flux across cell-free, coated control inserts was also measured. The apparent permeability coefficient (P_{app}) was calculated from the concentration difference of the tracer in the abluminal compartments ($\Delta[C]_A$) after 1 hour (Δt) and luminal compartments at 0 hour ($[C]_L$), the volume of the abluminal compartment (V_A; 1.5 mL) and the surface area available for permeability (A; 1.1 cm^2) by the following equation [66].

$$P^{app}\left(\frac{cm}{s}\right) = \frac{\Delta[C]^A * V^A}{A * [C]^L * \Delta t}$$

4.7 Transport and uptake studies

TEER was measured at room temperature prior to all experiments, using an Endohm-12 cup electrode chamber (World Precision Instruments, Sarasota, Florida) connected to a Millicell-ERS device (Millipore, Massachusetts, USA). Cells were subsequently equilibrated to 37°C before initiating transport or uptake experiments. Transcellular transport studies were performed directly in the culture medium after 3 days of co-culture. The radioisotopes ^{3}H-digoxin, ^{3}H-D-glucose, and ^{3}H-L-leucine were purchased from Perkin Elmer (Hvidovre, Denmark). Zosuquidar hydrochloride, unlabelled D-glucose, and BCH were from Sigma-Aldrich (Steinheim, Germany).

The experiments were initiated by adding a trace solution (1 µCi/ml ^{3}H-digoxin and 0.5 µCi/ml ^{14}C-D-mannitol) to either the apical or basolateral medium. Culture trays were placed on a temperature-controlled shaking table at 37°C, 90 rpm. Receiver samples (50 µl from the apical or 100 µl from the basolateral compartment) were withdrawn after 15, 30, 45, 60, 75, and 90 minutes and a donor sample was taken after 90 minutes (to confirm mass balance). Receiver samples were replaced with pre-heated (37°C) culture medium to maintain a constant volume. Transport studies were performed in both the apical-to-basolateral (A – B) and basolateral-to-apical (B – A) direction. P-glycoprotein functionality was evaluated by co-application of zosuquidar (0.5 µM) in both apical and basolateral compartments.

Uptake studies were performed in Hank's balanced salt solution with Ca^{2+}/Mg^{2+} (HBSS) with HEPES (10 mM), 0.05% BSA either with (for leucine uptake) or without glucose (for glucose uptake). The culture medium was removed and cells were washed twice with HBSS and subsequently incubated 10 minutes at 37°C with fresh HBSS with or without the LAT-1 inhibitor, BCH (100 µM) in both compartments (for leucine uptake). The experiments were initiated by adding the trace solution (1 µCi/ml ^{3}H-D-glucose or 1 µCi/ml ^{3}H-L-leucine) to the apical compartment. Then, cells were incubated for 2 minutes for glucose uptake and 5 minutes for leucine uptake. Receiver and donor samples were withdrawn at the end of the uptake study and the trace solution was removed. The cells were washed three times in ice-cold HBSS and the permeable supports were cut out and put into scintillation vials. The concentration dependency of glucose uptake was investigated by co-administration of 2 mM unlabelled D-glucose.Samples were transferred to Ultima Gold scintillation fluid (Perkin-Elmer) and radioactivity was counted in a Tri-Carb 2100 TR Liquid Scintillation Analyzer (Packard Instrument Company, Meriden, USA).

The measured molar amounts in the receiver samples from the transport studies were corrected for the dilution from replacing the receiver samples using equation 1:

$$Mass_{total} = V_s \times \left(\sum_{n=1} C_{n-1} \right) + C_n \times V_t$$

V_s is the volume of the receiver samples, V_t is the total volume of the receiver solution and C_n is the concentration of the isotope in the receiver sample, n. The corrected amount transported was plotted as the total amount transported per cm^2 per unit of time. Fluxes (J) were calculated from the steady-state slopes of the straight lines. Apparent permeability values were calculated using equation 2:

$$P_{app} = \frac{J_{ss}}{C_{donor}}$$

P_{app} is the apparent permeability, J_{ss} is the observed steady-state flux and C_{donor} is the concentration in the donor compartment after spiking. Efflux ratios were calculated as the apparent permeability in the B – A direction divided by the apparent permeability in the A – B direction. Digoxin permeability and efflux ratios were analysed using one-way analysis of variance followed by Tukey's test for multiple comparisons ($\alpha = 0.05$). Concentration dependency of D-glucose uptake and BCH inhibition of leucine uptake were examined using a two-sided Student's t-test ($\alpha = 0.05$).

4.8 RT-qPCR analysis

For real-time quantitative PCR (RT-qPCR), astrocytes and pericytes were cultured in T75 flasks and BECs were co-cultured with astrocytes on 75 mm diameter polycarbonate Transwell® inserts (Costar, Corning) as it is described in '*In vitro* BBB model constraction'. The cells were washed twice with ice-cold PBS and collected. Total RNA was extracted using the NucleoSpin® RNA Isolation Kit (Macherey-Nagel, Düren, Germany) according to the manufacturer's instructions. Material from one T75 flask or one insert was used to generate each RNA sample. The mRNA-purity was measured using NanoDrop 2000c UV-VIS Spectrophotometer (ThermoFisher Scientific, Waltham, MA, USA). Only mRNA samples with a 260/280 ratio over 2.00 were used for further analysis. Primers were designed using SDSC BiologyWorkbench and NCBI and retrieved from Thermo Fisher Scientific. Reverse transcription of mRNA was performed using High CapacitycDNA reverse transcription kit (4368814) from Thermo FisherScientific, according to the manufacturer's protocol. Riboloc R1 (Thermo Scientific) was used as RNAse inhibitor. PTC-200 ThermalCycler (MJ Research) was used for reverse transcription of mRNA to cDNA. The following primer pairs were used: Sortilin fwd 5'-AGACATCCTTGAGCGCAACT-3', rvs

5’-CGTAGCCGTAGGAACTGCTC-3’, product size 123 bps; Glyceraldehyde-3-Phosphate Dehydrogenase (GAPDH) fwd 5’-AGACAGCCGCATCTTCTTGT-3’, rvs 5’-CTTGCCGTGGGTAGAGTCAT-3’, product size 207 bps; β-actin fwd 5’-TGTCACCAACTGGGACGATA-3’, rvs 5’-CTGGGTCATCTTTTCACGGT-3’, product size 139 bps. Primer efficiencies were calculated by the equation E = 10(−1/slope), where the slope was found from a ten-fold serial dilutions calibration curve. Primer pairs were accepted if the efficiencies were in the range of 1.9–2.1 and obtained regular melting curves. RT-qPCR analysis was performed using Light Cycler 96 Instrument (Roche, Basel, Switzerland), and cDNA corresponding to 0.31 µg RNA per reaction was used. A reaction mixture of 20 µl consisting of 2 µl cDNA, 5 µl primer (a mix containing 2 µM of forward and reverse primers), 3 µl water (PCR-grade), and 10 µl mastermix was used in the PCR. Cycling conditions were as follows: pre-incubation at 95°C for 600 s, 45 cycles 95°C for 10 s, 55°C for 10 s, and 72°C for 20 s. Melting curves were determined for all samples to verify the specificity of amplicons. All samples were run in triplicates. All PCR data was normalized to the geomean of reference genes β-actin and GAPDH. Genes above 35 average cycle-threshold value were considered to be not expressed.

4.9 Western blot

For cell lysates, cells were washed with PBS and lysed in ExB lysis buffer (150 mM NaCl, 20 mM $MgCl_2$, 20 mM $CaCl_2$, 100 mM HEPES, 1% TritonX-100, complete™ p
rotease inhibitor). 5 µg of each protein sample was loaded on a 4-12% polyacrylamide gel (GeneScript, New Jersey, USA) and subsequently transferred to nitrocellulose membrane or polyvinylidene (Invitrogen iBlot). To improve the signals of Akt and phospho-Akt protein, the polyvinylidene membranes were incubated with 4% paraformaldehyde in PBS for 30 min at RT and boiled for 5 min in PBS. Before incubating with primary antibodies overnight at 4°C, the membrane was blocked in 5% skimmed milk, 0.01 M Tris-HCl, 0.15 M NaCl, and 0.1% Tween 20, pH 7.6 in buffer solution. The primary antibodies were: anti-sortilin antibody (AF2934, 1:1000; R&D Systems, Minneapolis, MN, USA), anti-claudin 5 antibody (SAB4502981, 1:1000), anti-ZO-1 antibody (61-7300, 1:250; Invitrogen, Carlsbad, CA, USA), anti-β-catenin antibody (610153, 1:1000; BD Transduction Laboratories, San Diego, CA, USA), anti-VE-cadherin antibody (36-1900, 1:500; Invitrogen), anti-phospho-Akt antibody (4060, 1:1000; Cell Signaling Techonology, Danvers, MA, USA), anti-Akt antibody (9272, 1:1000; Cell Signaling Techonology), anti-phospho-p44/42 MAPK (Erk1/2) antibody (4695, 1:1000; Cell Signaling

Techonology), anti-p44/42 MAPK (Erk1/2) antibody (9101, 1:1000; Cell Signaling Techonology), anti-β-actin antibody (A5441, 1:1000), anti-β-tubulin antibody (STJ31562, 1:1000; St. John's Lab, London, UK) and anti-GAPDH antibody (G8795, 1:1000). Secondary horseradish peroxidase (HRP)-conjugated anti goat IgG or anti-rabbit IgG or anti-mouse IgG antibodies (1:2000) were applied for 1 hour at room temperature. Finally, bands were detected using ECL (GE Healthcare) or SuperSignal (Thermo scientific, Rockford, USA) according to the manufacturer's recommendations and visualised using LAS 4000 (Fujifilm). ImageJ software was used to perform densitometry analyses of Western blot results on unprocessed images. For representative Western blot pictures to improve clarity, brightness, and contrast adjustment were applied equally across the entire image. The unprocessed pictures are uploaded as a source data file.

4.10 Immunohistochemistry

Brains (n = 6) for albumin-immunohistochemistry were cut into 3 smaller pieces and fixed in 4% paraformaldehyde dissolved in 0.01 M potassium phosphate-buffered saline (KPBS) pH 7.4 for two days. Then, the fixed brains were cut frontally on a cryostat at 40 µm sequentially in a series of six and collected free-floating in KPBS pH 7.4. To block unspecific bindings, sections were incubated in a blocking buffer consisting of 3% swine serum, 0.3% Triton X-100 diluted in 0.01 M KPBS. These sections were then incubated with the primary antibody rabbit anti-albumin (A001, 1:200; Dako, Glostrup, Denmark) diluted in blocking buffer overnight at 4°C. The next day, the sections were incubated with the secondary antibody swine anti-rabbit immunoglobulin (E00353, 1:200; Dako, Glostrup, Denmark) diluted in blocking buffer. Binding of the antibodies was subsequently visualised using the ABC system and 3,3′-diaminobenzidine tetrahydrochloride (DAB) [67]. The brain sections were mounted on cover glasses and visualized using the Axiovert 2000 (Carl-Zeiss) microscope. Image analysis was performed using ImageJ 1.47V.

4.11 Transmission electronmicroscopy (TEM)

For TEM, the deeply anesthetized animals were perfusion fixed with a solution of 2% glutaraldehyde, 4% paraformaldehyde in 0.1 M Na-cacodylate buffer pH 7.4. After perfusion, the brains were excised and placed in the fixative solution to await further processing. The cortex was removed from the rest of the brain and cut into 1 mm^3 pieces. These pieces were washed 3 times in 0.1 M Na-cacodylate buffer and stained in a 1% osmium tetroxide in 0.1 M Na-cacodylate buffer solution for 1 hour at room temperature. Following staining with osmium tetroxide, the samples

were washed 3 times in milliQ water and suspended in a 1% uranyl acetate solution overnight. The following day, samples were washed twice in milliQ water followed by dehydration in increasing concentrations of ethanol, 50%, 70%, 95%, 100%, and 100% with 10 minutes between solvent exchanges. The samples were further dehydrated 3 times in acetonitrile for 5 minutes each before the start of resin infiltration. The samples were placed in a 1:1 solution of agar 100 medium hardness embedding resin and acetonitrile. After 1 hour, the samples were placed in a 2:1 resin:acetonitrile solution and the resin was allowed to infiltrate overnight. The next morning, the samples were suspended in pure resin for 2 hours before being placed in BEEM capsules and cured at 60°C for 24 hours. After the resin was completely cured, resin blocks were removed from the oven and the block face was roughly trimmed with a razor blade to expose the tissue surface. Using an RMC-7 ultramicrotome with a diamond knife, 100 nm thick sections of brain tissue were cut and placed on 200 mesh formvar coated nickel grids. TEM was performed utilizing an FEI Tecnai T12 Biotwin TEM operating at 120 kV located at the Center for Electron Nanoscopy at the Technical University of Denmark, and images were acquired using a Bottom mounted CCD, Gatan Orius SC1000WC. A minimum of 50 capillaries was imaged for each sample. Additionally, endothelial wall thickness was measured.

4.12 Immunocytochemistry and confocal microscopy

For immunocytochemistry, BECs were grown on polycarbonate Transwell® filter inserts in co-culture with astrocytes. Astrocytes and pericytes were cultured on coated cover glasses as described above. Confluent cell layers were fixed with 4% paraformaldehyde in PBS for 20 min at RT. For permeabilization 0.2% Triton X-100 in PBS for 10 min were used followed by blocking of samples in 2% BSA in PBS for 20 min. Primary antibodies and secondary antibodies were diluted in 1.5% BSA and 0.05% Triton X-100. The following primary antibodies were applied for 1 hour at room temperature: anti-sortilin antibody (AF2934, 1:300; R&D Systems, Minneapolis, MN, USA), anti-M6PR antibody (ab134153, 1:100, Abcam, Cambridge, UK), anti-claudin 5 antibody (SAB4502981, 1:300), anti-ZO-1 antibody (61-7300, 1:300; Invitrogen, Carlsbad, CA, USA), anti-β-catenin antibody (610153, 1:300; BD Transduction Laboratories, San Diego, CA, USA), anti-VE-cadherin antibody (36-1900, 1:300; Invitrogen), anti-GFAP (GA5) antibody (3670, 1:200; Cell Signaling Techonology, Danvers, MA, USA) and anti-NG2 antibody (ab83178, 1:200; Abcam, Cambridge, UK). Secondary Alexa Fluor-488 conjugated anti-goat or Alexa Fluor-568 conjugated anti-mouse or anti rabbit antibodies (1:500) were applied for 1 hour at room

temperature. For staining of nuclei, Hoechst 32528 (0.5 µg/ml) in distilled water for 10 min was applied as a separate step. In between the steps, samples were washed 3 times for 5 min in 0.02% Triton-X100 in PBS to remove unbound antibodies. Finally, samples were mounted on glass slides using Dako fluorescence mounting medium (Dako, Glostrup, Denmark). Confocal images were captured by Olympus IX-83 fluorescent microscope with Andor confocal spinning unit and Andor iXon Ultra 897 camera, Olympus UPlanSApo, 60x/1.20 NA water objective lens or Olympus UPlanFL N, 40x/1.30 NA oil objective lens, using Olympus CellSens software (Olympus). For representative images, the brightness and contrast adjustments were applied to the same extent for the WT and KO images using ImageJ software.

4.13 Line intensity scanning

Multichannel images were analysed using Fiji software. During line intensity scan analysis, the intensity parameters were counted on maximum intensity projections of confocal Z-stack images. Only images stained and captured in the same experiments were compared. Three-six images of randomly selected fields of the confluent BECs monolayer from each filter were acquired. On each image 3-5 cells were chosen to draw lines in the cytoplasm and at the cell border. To quantify the observed differences, the fluorescent intensities at the cell border and in the cytoplasm were measured. Then the fluorescent intensity at the cell border was divided by the measured fluorescent intensity in the cytoplasm on the same image. Here, we refer to the calculated fluorescent intensity ratio as localisation ratio. The calculation is summarized in the following equation:

$$\text{Localisation ratio} = \frac{\text{fluorescent intensity at the cell border}}{\text{fluorescent intensity in the cytoplasm}}$$

The localisation ratios were compared between the WT-BECs and KO-BECs.

Additionally, the measured fluorescent intensity values either at the cell border or in the cytoplasm were compared between the WT- and the KO-groups from the same experiment. Similarly, the measured fluorescent intensity values of the cytoplasm in the same experiment were compared between the two groups. The values are shown as a/the percentage of the WT-group (100%).

4.14 Statistical analyses

All curve fitting and statistical analyses were performed in Graph Pad Prism version 6 (GraphPad Software, La Jolla, CA, USA). All *in vitro* studies were performed in three individual models (biological replicates) with every 3 permeable supports for each condition within each model. Data are reported as means ± standard error of the mean (SEM).

Author contributions

Conceptualization; A.E.T. and M.S.N.; data curation; A.E.T., P.L.M., and M.N.; formal analysis A.E.T., H.C.H., C.G., K.B.J.; funding acquisition M.S.N.; investigation A.E.T., A.H., A.K., D.V.L., H.C.H., C.G., A.B., M.S.T., K.B.J., T.M., and P.J.K.; methodology – A.E.T., A.H., H.C.H., C.G., A.B., M.S.T., K.B.J., and P.K.; project administration A.E.T. and M.S.N.; resources M.S.N., supervision, T.L.A. M.N., T.M., B.B., A.E.T. and M.S.N.; visualization A.E.T., M.S.T., and P.K.; writing A.E.T., A.H., H.C.H., C.G., M.S.T., P.K., T.M., B.B. and M.S.N. All authors have read and approved the final manuscript.

Acknowledgements

Annemette B. Marnow is thanked for expert technical assistance. This work has received support from the Research Initiative on Brain Barriers and Drug Delivery funded by the Lundbeck Foundation (Grant no. 2013-14113) and the EU/EFPIA Innovative Medicines Initiative Joint Undertaking IM2PACT (Grant No. 807015). The funders had no role in study design, data collection, and interpretation, or the decision to submit the work for publication.

References

1. Abbott, N. J., Patabendige, A. A., Dolman, D. E., Yusof, S. R. & Begley, D. J. (2010) Structure and function of the blood-brain barrier, *Neurobiol Dis.* **37**, 13-25.

2. Worzfeld, T. & Schwaninger, M. (2016) Apicobasal polarity of brain endothelial cells, *J Cereb Blood Flow Metab.* **36**, 340-62.

3. Stewart, P. A., Beliveau, R. & Rogers, K. A. (1996) Cellular localization of P-glycoprotein in brain versus gonadal capillaries, *J Histochem Cytochem.* **44**, 679-85.

4. Gerhart, D. Z., LeVasseur, R. J., Broderius, M. A. & Drewes, L. R. (1989) Glucose transporter localization in brain using light and electron immunocytochemistry, *J Neurosci Res.* **22**, 464-72.

5. Duelli, R., Enerson, B. E., Gerhart, D. Z. & Drewes, L. R. (2000) Expression of large amino acid transporter LAT1 in rat brain endothelium, *J Cereb Blood Flow Metab.* **20**, 1557-62.

6. Stamatovic, S. M., Johnson, A. M., Keep, R. F. & Andjelkovic, A. V. (2016) Junctional proteins of the blood-brain barrier: New insights into function and dysfunction, *Tissue Barriers.* **4**, e1154641.

7. Ohtsuki, S., Yamaguchi, H., Katsukura, Y., Asashima, T. & Terasaki, T. (2008) mRNA expression levels of tight junction protein genes in mouse brain capillary endothelial cells highly purified by magnetic cell sorting, *J Neurochem.* **104**, 147-54.

8. Crosby, C. V., Fleming, P. A., Argraves, W. S., Corada, M., Zanetta, L., Dejana, E. & Drake, C. J. (2005) VE-cadherin is not required for the formation of nascent blood vessels but acts to prevent their disassembly, *Blood.* **105**, 2771-6.

9. Itoh, M., Nagafuchi, A., Moroi, S. & Tsukita, S. (1997) Involvement of ZO-1 in cadherin-based cell adhesion through its direct binding to alpha catenin and actin filaments, *J Cell Biol.* **138**, 181-92.

10. Itoh, M., Furuse, M., Morita, K., Kubota, K., Saitou, M. & Tsukita, S. (1999) Direct binding of three tight junction-associated MAGUKs, ZO-1, ZO-2, and ZO-3, with the COOH termini of claudins, *J Cell Biol.* **147**, 1351-63.

11. Engelhardt, B. & Liebner, S. (2014) Novel insights into the development and maintenance of the blood-brain barrier, *Cell Tissue Res.* **355**, 687-99.

12. Cong, X. & Kong, W. (2020) Endothelial tight junctions and their regulatory signaling pathways in vascular homeostasis and disease, *Cell Signal.* **66**, 109485.

13. Gonzalez-Mariscal, L., Tapia, R. & Chamorro, D. (2008) Crosstalk of tight junction components with signaling pathways, *Biochim Biophys Acta.* **1778**, 729-56.

14. Coutinho, M. F., Prata, M. J. & Alves, S. (2012) A shortcut to the lysosome: the mannose-6-phosphate-independent pathway, *Mol Genet Metab.* **107**, 257-66.

15. Petersen, C. M., Nielsen, M. S., Nykjaer, A., Jacobsen, L., Tommerup, N., Rasmussen, H. H., Roigaard, H., Gliemann, J., Madsen, P. & Moestrup, S. K. (1997) Molecular identification of a novel candidate sorting receptor purified from human brain by receptor-associated protein affinity chromatography, *J Biol Chem.* **272**, 3599-605.

16. Nielsen, M. S., Madsen, P., Christensen, E. I., Nykjaer, A., Gliemann, J., Kasper, D., Pohlmann, R. & Petersen, C. M. (2001) The sortilin cytoplasmic tail conveys Golgi-endosome transport and binds the VHS domain of the GGA2 sorting protein, *EMBO J.* **20**, 2180-90.

17. Nykjaer, A., Lee, R., Teng, K. K., Jansen, P., Madsen, P., Nielsen, M. S., Jacobsen, C., Kliemannel, M., Schwarz, E., Willnow, T. E., Hempstead, B. L. & Petersen, C. M. (2004) Sortilin is essential for proNGF-induced neuronal cell death, *Nature.* **427**, 843-8.

18. Shi, J. & Kandror, K. V. (2007) The luminal Vps10p domain of sortilin plays the predominant role in targeting to insulin-responsive Glut4-containing vesicles, *J Biol Chem.* **282**, 9008-16.

19. Al-Yozbaki, M., Acha-Sagredo, A., George, A., Liloglou, T. & Wilson, C. M. (2020) Balancing neurotrophin pathway and sortilin function: Its role in human disease, *Biochim Biophys Acta Rev Cancer.* **1874**, 188429.

20. Carlo, A. S., Nykjaer, A. & Willnow, T. E. (2014) Sorting receptor sortilin-a culprit in cardiovascular and neurological diseases, *J Mol Med (Berl).* **92**, 905-11.

21. Kjolby, M., Nielsen, M. S. & Petersen, C. M. (2015) Sortilin, encoded by the cardiovascular risk gene SORT1, and its suggested functions in cardiovascular disease, *Curr Atheroscler Rep.* **17**, 496.

22. Willnow, T. E., Petersen, C. M. & Nykjaer, A. (2008) VPS10P-domain receptors - regulators of neuronal viability and function, *Nat Rev Neurosci.* **9**, 899-909.

23. Zhang, Y., Chen, K., Sloan, S. A., Bennett, M. L., Scholze, A. R., O'Keeffe, S., Phatnani, H. P., Guarnieri, P., Caneda, C., Ruderisch, N., Deng, S., Liddelow, S. A., Zhang, C., Daneman, R., Maniatis, T., Barres, B. A. & Wu, J. Q. (2014) An RNA-sequencing transcriptome and splicing database of glia, neurons, and vascular cells of the cerebral cortex, *J Neurosci.* **34**, 11929-47.

24. Zhang, Y., Sloan, S. A., Clarke, L. E., Caneda, C., Plaza, C. A., Blumenthal, P. D., Vogel, H., Steinberg, G. K., Edwards, M. S., Li, G., Duncan, J. A., 3rd, Cheshier, S. H., Shuer, L. M., Chang,

E. F., Grant, G. A., Gephart, M. G. & Barres, B. A. (2016) Purification and Characterization of Progenitor and Mature Human Astrocytes Reveals Transcriptional and Functional Differences with Mouse, *Neuron.* **89**, 37-53.

25. Vanlandewijck, M. & Betsholtz, C. (2018) Single-Cell mRNA Sequencing of the Mouse Brain Vasculature, *Methods Mol Biol.* **1846**, 309-324.

26. Zhang, Y., Chen, K., Sloan, S. A., Bennett, M. L., Scholze, A. R., O'Keeffe, S., Phatnani, H. P., Guarnieri, P., Caneda, C., Ruderisch, N., Deng, S., Liddelow, S. A., Zhang, C., Daneman, R., Maniatis, T., Barres, B. A. & Wu, J. Q. (2014) Brain RNA-Seq in

27. Vanlandewijck, M. & Betsholtz, C. (2018) Vascular single cells in

28. Toth, A. E., Siupka, P., TJ, P. A., Veno, S. T., Thomsen, L. B., Moos, T., Lohi, H. T., Madsen, P., Lykke-Hartmann, K. & Nielsen, M. S. (2018) The Endo-Lysosomal System of Brain Endothelial Cells Is Influenced by Astrocytes In Vitro, *Mol Neurobiol.* **55**, 8522-8537.

29. Nakagawa, S., Deli, M. A., Kawaguchi, H., Shimizudani, T., Shimono, T., Kittel, A., Tanaka, K. & Niwa, M. (2009) A new blood-brain barrier model using primary rat brain endothelial cells, pericytes and astrocytes, *Neurochem Int.* **54**, 253-63.

30. Goncalves, N. P., Yan, Y., Ulrichsen, M., Veno, M. T., Poulsen, E. T., Enghild, J. J., Kjems, J. & Vaegter, C. B. (2020) Modulation of Small RNA Signatures in Schwann-Cell-Derived Extracellular Vesicles by the p75 Neurotrophin Receptor and Sortilin, *Biomedicines.* **8**.

31. Johnsen, K. B., Burkhart, A., Melander, F., Kempen, P. J., Vejlebo, J. B., Siupka, P., Nielsen, M. S., Andresen, T. L. & Moos, T. (2017) Targeting transferrin receptors at the blood-brain barrier improves the uptake of immunoliposomes and subsequent cargo transport into the brain parenchyma, *Sci Rep.* **7**, 10396.

32. Plateel, M., Teissier, E. & Cecchelli, R. (1997) Hypoxia dramatically increases the nonspecific transport of blood-borne proteins to the brain, *J Neurochem.* **68**, 874-7.

33. Srinivasan, B., Kolli, A. R., Esch, M. B., Abaci, H. E., Shuler, M. L. & Hickman, J. J. (2015) TEER measurement techniques for in vitro barrier model systems, *J Lab Autom.* **20**, 107-26.

34. Lochhead, J. J., Yang, J., Ronaldson, P. T. & Davis, T. P. (2020) Structure, Function, and Regulation of the Blood-Brain Barrier Tight Junction in Central Nervous System Disorders, *Front Physiol.* **11**, 914.

35. Mazella, J., Petrault, O., Lucas, G., Deval, E., Beraud-Dufour, S., Gandin, C., El-Yacoubi, M., Widmann, C., Guyon, A., Chevet, E., Taouji, S., Conductier, G., Corinus, A., Coppola, T., Gobbi, G., Nahon, J. L., Heurteaux, C. & Borsotto, M. (2010) Spadin, a sortilin-derived peptide, targeting

rodent TREK-1 channels: a new concept in the antidepressant drug design, *PLoS Biol.* **8**, e1000355.

36. Sarret, P., Krzywkowski, P., Segal, L., Nielsen, M. S., Petersen, C. M., Mazella, J., Stroh, T. & Beaudet, A. (2003) Distribution of NTS3 receptor/sortilin mRNA and protein in the rat central nervous system, *J Comp Neurol.* **461**, 483-505.

37. Helms, H. C., Abbott, N. J., Burek, M., Cecchelli, R., Couraud, P. O., Deli, M. A., Forster, C., Galla, H. J., Romero, I. A., Shusta, E. V., Stebbins, M. J., Vandenhaute, E., Weksler, B. & Brodin, B. (2016) In vitro models of the blood-brain barrier: An overview of commonly used brain endothelial cell culture models and guidelines for their use, *J Cereb Blood Flow Metab.* **36**, 862-90.

38. Yu, F., Liu, Y. & Xu, J. (2018) Pro-BDNF Contributes to Hypoxia/Reoxygenation Injury in Myocardial Microvascular Endothelial Cells: Roles of Receptors p75(NTR) and Sortilin and Activation of JNK and Caspase 3, *Oxid Med Cell Longev.* **2018**, 3091424.

39. Bao, J. X., Jin, S., Zhang, F., Wang, Z. C., Li, N. & Li, P. L. (2010) Activation of membrane NADPH oxidase associated with lysosome-targeted acid sphingomyelinase in coronary endothelial cells, *Antioxid Redox Signal.* **12**, 703-12.

40. Glerup, S., Lume, M., Olsen, D., Nyengaard, J. R., Vaegter, C. B., Gustafsen, C., Christensen, E. I., Kjolby, M., Hay-Schmidt, A., Bender, D., Madsen, P., Saarma, M., Nykjaer, A. & Petersen, C. M. (2013) SorLA controls neurotrophic activity by sorting of GDNF and its receptors GFRalpha1 and RET, *Cell Rep.* **3**, 186-99.

41. Siao, C. J., Lorentz, C. U., Kermani, P., Marinic, T., Carter, J., McGrath, K., Padow, V. A., Mark, W., Falcone, D. J., Cohen-Gould, L., Parrish, D. C., Habecker, B. A., Nykjaer, A., Ellenson, L. H., Tessarollo, L. & Hempstead, B. L. (2012) ProNGF, a cytokine induced after myocardial infarction in humans, targets pericytes to promote microvascular damage and activation, *J Exp Med.* **209**, 2291-305.

42. Schmidt, V. & Willnow, T. E. (2016) Protein sorting gone wrong--VPS10P domain receptors in cardiovascular and metabolic diseases, *Atherosclerosis.* **245**, 194-9.

43. Huang, G. R., Buckler-Pena, D., Nauta, T., Singh, M., Asmar, A., Shi, J., Kim, J. Y. & Kandror, K. V. (2013) Insulin responsiveness of glucose transporter 4 in 3T3-L1 cells depends on the presence of sortilin, *Molecular Biology of the Cell.* **24**, 3115-3122.

44. Pardridge, W. M., Boado, R. J. & Farrell, C. R. (1990) Brain-type glucose transporter (GLUT-1) is selectively localized to the blood-brain barrier. Studies with quantitative western blotting and in situ hybridization, *J Biol Chem.* **265**, 18035-40.

45. Zipser, B. D., Johanson, C. E., Gonzalez, L., Berzin, T. M., Tavares, R., Hulette, C. M., Vitek, M. P., Hovanesian, V. & Stopa, E. G. (2007) Microvascular injury and blood-brain barrier leakage in Alzheimer's disease, *Neurobiol Aging.* **28**, 977-86.

46. Kalayci, R., Kaya, M., Uzun, H., Bilgic, B., Ahishali, B., Arican, N., Elmas, I. & Kucuk, M. (2009) Influence of hypercholesterolemia and hypertension on the integrity of the blood-brain barrier in rats, *Int J Neurosci.* **119**, 1881-904.

47. Acharya, N. K., Levin, E. C., Clifford, P. M., Han, M., Tourtellotte, R., Chamberlain, D., Pollaro, M., Coretti, N. J., Kosciuk, M. C., Nagele, E. P., Demarshall, C., Freeman, T., Shi, Y., Guan, C., Macphee, C. H., Wilensky, R. L. & Nagele, R. G. (2013) Diabetes and hypercholesterolemia increase blood-brain barrier permeability and brain amyloid deposition: beneficial effects of the LpPLA2 inhibitor darapladib, *J Alzheimers Dis.* **35**, 179-98.

48. Ruan, C. S., Liu, J., Yang, M., Saadipour, K., Zeng, Y. Q., Liao, H., Wang, Y. J., Bobrovskaya, L. & Zhou, X. F. (2018) Sortilin inhibits amyloid pathology by regulating non-specific degradation of APP, *Exp Neurol.* **299**, 75-85.

49. Musunuru, K., Strong, A., Frank-Kamenetsky, M., Lee, N. E., Ahfeldt, T., Sachs, K. V., Li, X., Li, H., Kuperwasser, N., Ruda, V. M., Pirruccello, J. P., Muchmore, B., Prokunina-Olsson, L., Hall, J. L., Schadt, E. E., Morales, C. R., Lund-Katz, S., Phillips, M. C., Wong, J., Cantley, W., Racie, T., Ejebe, K. G., Orho-Melander, M., Melander, O., Koteliansky, V., Fitzgerald, K., Krauss, R. M., Cowan, C. A., Kathiresan, S. & Rader, D. J. (2010) From noncoding variant to phenotype via SORT1 at the 1p13 cholesterol locus, *Nature.* **466**, 714-9.

50. Bi, L., Chiang, J. Y., Ding, W. X., Dunn, W., Roberts, B. & Li, T. (2013) Saturated fatty acids activate ERK signaling to downregulate hepatic sortilin 1 in obese and diabetic mice, *J Lipid Res.* **54**, 2754-62.

51. Demont, Y., Corbet, C., Page, A., Ataman-Onal, Y., Choquet-Kastylevsky, G., Fliniaux, I., Le Bourhis, X., Toillon, R. A., Bradshaw, R. A. & Hondermarck, H. (2012) Pro-nerve growth factor induces autocrine stimulation of breast cancer cell invasion through tropomyosin-related kinase A (TrkA) and sortilin protein, *J Biol Chem.* **287**, 1923-31.

52. Li, J., Matye, D. J. & Li, T. (2015) Insulin resistance induces posttranslational hepatic sortilin 1 degradation in mice, *J Biol Chem.* **290**, 11526-36.

53. Li, J., Chen, C., Li, Y., Matye, D. J., Wang, Y., Ding, W. X. & Li, T. (2017) Inhibition of insulin/PI3K/AKT signaling decreases adipose Sortilin 1 in mice and 3T3-L1 adipocytes, *Biochim Biophys Acta Mol Basis Dis.* **1863**, 2924-2933.

54. Hers, I., Vincent, E. E. & Tavare, J. M. (2011) Akt signalling in health and disease, *Cell Signal.* **23**, 1515-27.

55. Moelling, K., Schad, K., Bosse, M., Zimmermann, S. & Schweneker, M. (2002) Regulation of Raf-Akt Cross-talk, *J Biol Chem.* **277**, 31099-106.

56. Zimmermann, S. & Moelling, K. (1999) Phosphorylation and regulation of Raf by Akt (protein kinase B), *Science.* **286**, 1741-4.

57. Singh, A. K., Jiang, Y., Gupta, S. & Benlhabib, E. (2007) Effects of chronic ethanol drinking on the blood brain barrier and ensuing neuronal toxicity in alcohol-preferring rats subjected to intraperitoneal LPS injection, *Alcohol Alcohol.* **42**, 385-99.

58. Tan, X., Egami, H., Ishikawa, S., Kurizaki, T., Hirota, M. & Ogawa, M. (2005) Zonula occludens-1 (ZO-1) redistribution is involved in the regulation of cell dissociation in pancreatic cancer cells, *Dig Dis Sci.* **50**, 1402-9.

59. Miyamoto, N., de Kozak, Y., Jeanny, J. C., Glotin, A., Mascarelli, F., Massin, P., BenEzra, D. & Behar-Cohen, F. (2007) Placental growth factor-1 and epithelial haemato-retinal barrier breakdown: potential implication in the pathogenesis of diabetic retinopathy, *Diabetologia.* **50**, 461-70.

60. Jacob, C., Yang, P. C., Darmoul, D., Amadesi, S., Saito, T., Cottrell, G. S., Coelho, A. M., Singh, P., Grady, E. F., Perdue, M. & Bunnett, N. W. (2005) Mast cell tryptase controls paracellular permeability of the intestine. Role of protease-activated receptor 2 and beta-arrestins, *J Biol Chem.* **280**, 31936-48.

61. Lan, M., Kojima, T., Osanai, M., Chiba, H. & Sawada, N. (2004) Oncogenic Raf-1 regulates epithelial to mesenchymal transition via distinct signal transduction pathways in an immortalized mouse hepatic cell line, *Carcinogenesis.* **25**, 2385-95.

62. Sato, H., Oyanagi, J., Komiya, E., Ogawa, T., Higashi, S. & Miyazaki, K. (2014) Amino-terminal fragments of laminin gamma2 chain retract vascular endothelial cells and increase vascular permeability, *Cancer Sci.* **105**, 168-75.

63. Gunduz, D., Troidl, C., Tanislav, C., Rohrbach, S., Hamm, C. & Aslam, M. (2019) Role of PI3K/Akt and MEK/ERK Signalling in cAMP/Epac-Mediated Endothelial Barrier Stabilisation, *Front Physiol.* **10**, 1387.

64. Xue, M., Chow, S. O., Dervish, S., Chan, Y. K., Julovi, S. M. & Jackson, C. J. (2011) Activated protein C enhances human keratinocyte barrier integrity via sequential activation of epidermal growth factor receptor and Tie2, *J Biol Chem.* **286**, 6742-50.

65. Nakagawa, S., Deli, M. A., Nakao, S., Honda, M., Hayashi, K., Nakaoke, R., Kataoka, Y. & Niwa, M. (2007) Pericytes from brain microvessels strengthen the barrier integrity in primary cultures of rat brain endothelial cells, *Cell Mol Neurobiol.* **27**, 687-94.

66. Youdim, K. A., Avdeef, A. & Abbott, N. J. (2003) In vitro trans-monolayer permeability calculations: often forgotten assumptions, *Drug Discov Today.* **8**, 997-1003.

67. Moos, T. & Rosengren Nielsen, T. (2006) Ferroportin in the postnatal rat brain: implications for axonal transport and neuronal export of iron, *Semin Pediatr Neurol.* **13**, 149-57.

Figure Legends

Figure 1 - Sortilin is expressed in the cells of the brain microvessels in rat. A RT-PCR shows *Sort1* gene expression in brain endothelial cells (BECs), astrocytes and pericytes. B Western blot demonstrates sortilin protein in wild-type (WT) microvessels, BECs, astrocytes, and pericytes, but not in the respective *Sort1-/-* knock-out cells (KO). B-actin serves as a loading control. C Representative immunocytochemistry of sortilin and trans-Golgi network localized mannose 6-phosphate receptor (M6PR) in WT-BECs. D-G Double immunocytochemistry shows sortilin (green) in WT-BECs, -astrocytes, and -pericytes, but not in the respective KOs. Nuclei are labelled with blue. Sortilin gives a strong staining around the nucleus of the WT-cells. Scale bars: 20 µM. D-E Brain microvessels and BECs were identified by claudin-5 staining (red). F Astrocytes were labelled with glial fibrillary acidic protein (GFAP; red). G Pericytes were stained against neuron-glial antigen 2 (NG2; red). Magnification is 40x (C, F) and 60x (D-E). All cells were primary and purified from rat. Data information: Data are presented as mean ± SEM. n ≥ 3 cultures.

Figure 2 - The brain microvessels of WT- and KO-rats. A Permeability of microvessels for oxaliplatin in *Sort1-/-* knock-out (KO)-rats compared to the wild-type (WT) -rats (100%) *in vivo* (n = 11 rats for each genotype). The oxaliplatin content of the brain homogenate was plotted as a/the percentage of administrated dose (AD%). B Immunohistochemistry against albumin in WT- and KO-brain. The top panel shows representative images of the cortex. The bottom panel displays images of the choroid plexus. Scale bar: 20 µm. C Transmission electron micrographs of brain capillaries in the cortex of WT- and KO-rat. A: astrocytic endfeet, E: endothelial cell, P: pericyte, RBC: red blood cell. Scale bar: 1 µm. D Average endothelial thickness of brain capillaries measured on the transmission electron micrographs. (n = 4 rats/genotype) Data information: Data are presented as mean ± SEM. ns: not significant **P≤0.01 (Student's t-test).

Figure 3 - The integrity of the wild-type (WT-BBB) and *Sort1-/-* knock out blood-brain barrier (KO-BBB) *in vitro*. A In vitro BBB model set-ups. Wild-type brain endothelial cells (WT-BECs) were grown on permeable inserts in co-culture with WT-astrocytes at the bottom of the dish. On the same way, in the KO-BBB model *Sort1-/-* brain endothelial cells (KO-BECs) were kept together with KO-astrocytes. B Apparent permeability (P_{app}) of KO-BBB compared to the WT-BBB model. C Tightness of KO-BECs/KO-astrocytes and WT-BECs/KO-astrocytes

compared to the WT-BBB model. D Polarized efflux transport activity of P-glycoprotein. Transendothelial transport of ^{3}H-digoxin across the WT-and KO-BECs' monolayer in the abluminal-to-luminal (B-A) and luminal-to-abluminal direction with and without P-glycoprotein specific inhibitor (i). Efflux ratios are derived from the apparent substrate permeability. E Glucose transporter 1 dependent glucose uptake. The uptake of ^{3}H-glucose was low in both BBB models, which was not affected by adding unlabelled glucose for competition (c). F LAT-1 dependent leucine uptake. LAT1 shows functional transport of ^{3}H-L-leucine and the transport that was inhibited by the LAT1 specific inhibitor (i). Data information: In (B-F) data are presented as mean ± SEM. n ≥ 3 cultures. ns: not significant, *P≤0.05, **P≤0.01, ***P≤0.001 (Student's t-test (B-C) and one-way ANOVA (D-F)).

Figure 4 - Immunocytochemistry and western blot for tight and adherent junctional proteins. A, C, E, G Immunocytochemistry and localisation ratio of zonula occludens-1 (A), claudin-5 (C), β-catenin (E), VE-cadherin (G). Nuclei are blue and sortilin is labeled with green. Magnification is 60x. Scale bars: 20 μM. B, D, F, H Quantitative Western blot analysis of zonula occludens-1 (B)**,** claudin-5 (D)**,** β-catenin (F)**,** VE-cadherin (H). BECs: brain endothelial cells, WT: wild type, KO: *Sort1-/-*. Data information: Data are presented as mean ± SEM. n ≥ 3 cultures. ns: not significant, *P≤0.05, **P≤0.01 (Student's t-test).

Figure 5 - Akt and MAPK signaling pathways. A, B Quantitative Western blot analysis of phospho-Akt (pAkt) and total Akt (T-Akt) (A), phospho-ERK1/2 (pERK1/2) and total ERK1/2 (T-ERK1/2) (B) and their ratios in the wild type (WT) and *Sort1-/-* (KO) brain endothelial cells. C Westen blot analysis of pAkt and total Akt in WT brain endothelial cells treated 1 hour with spadin (100 nM) or Akt-inhibitor (Akti-1/2; 10 μM). Apparent permeability (P_{app}) and localisation ratio of VE-cadherin protein in WT brain endothelial cells treated with Akti-1/2. The control group received culture medium. Data information: Data are presented as mean ± SEM. n ≥ 3 cultures. ns: not significant, *P≤0.05, **P≤0.01 (Student's t-test).

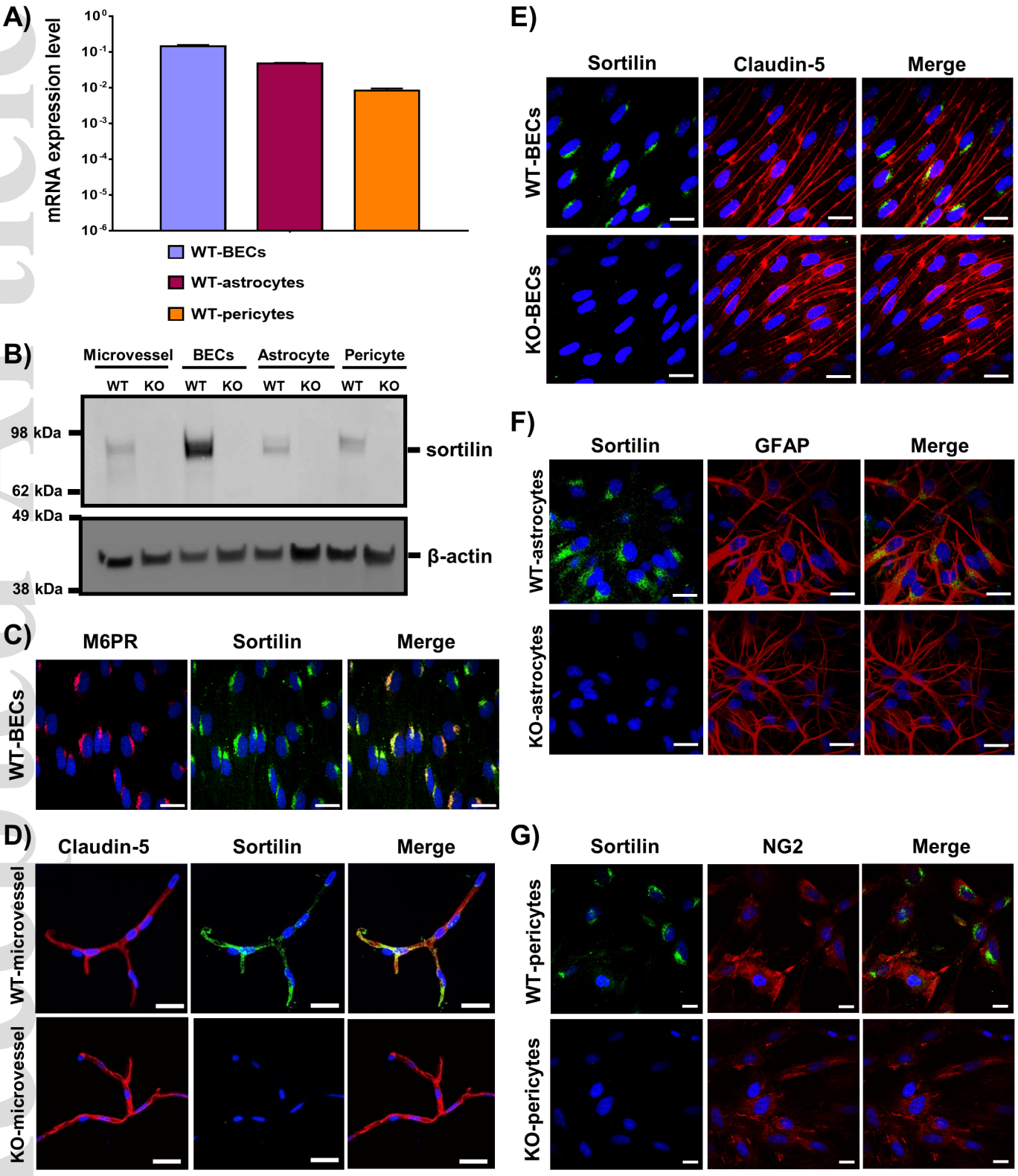

febs_16225_f1.tif

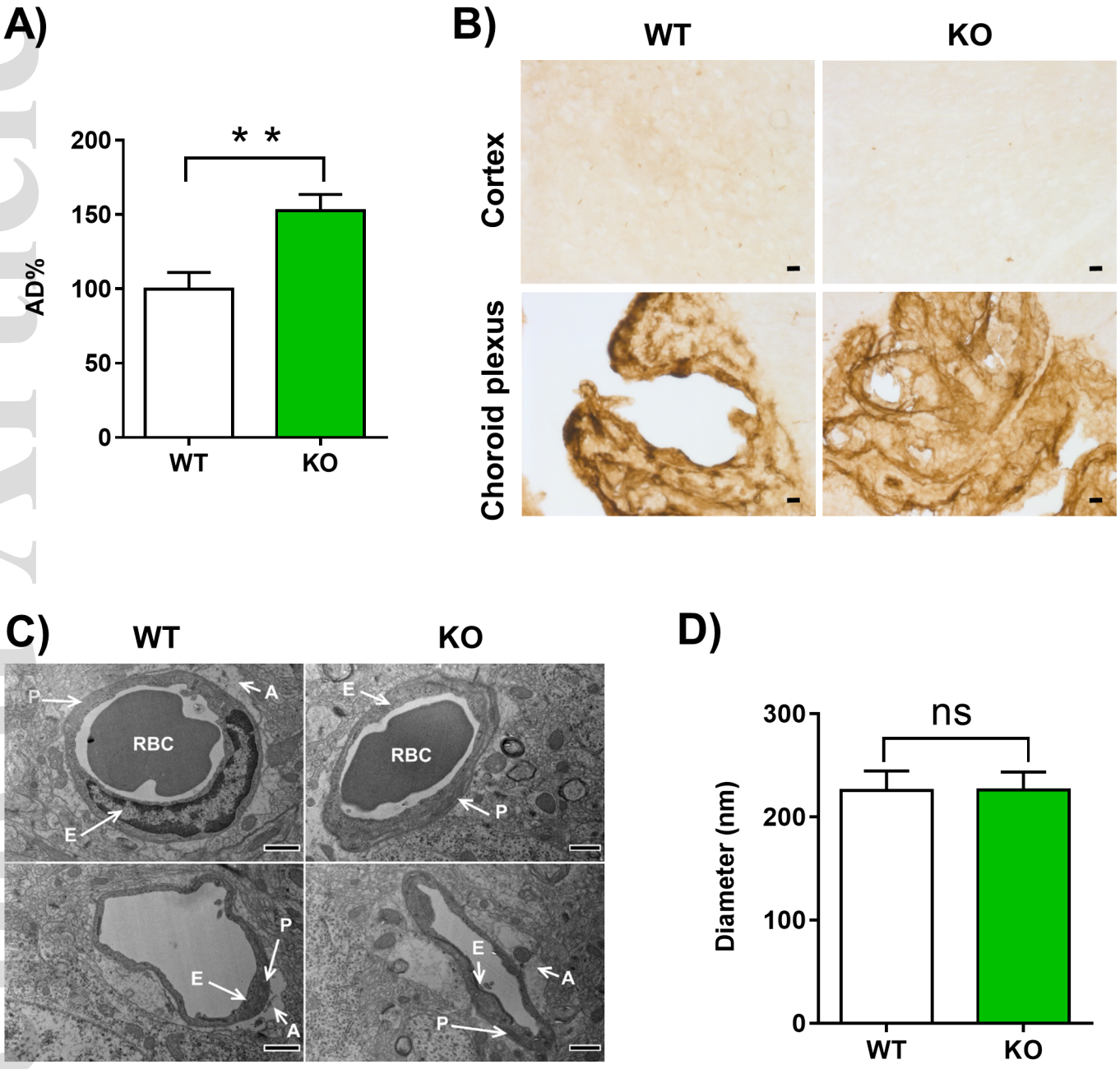

febs_16225_f2.tif

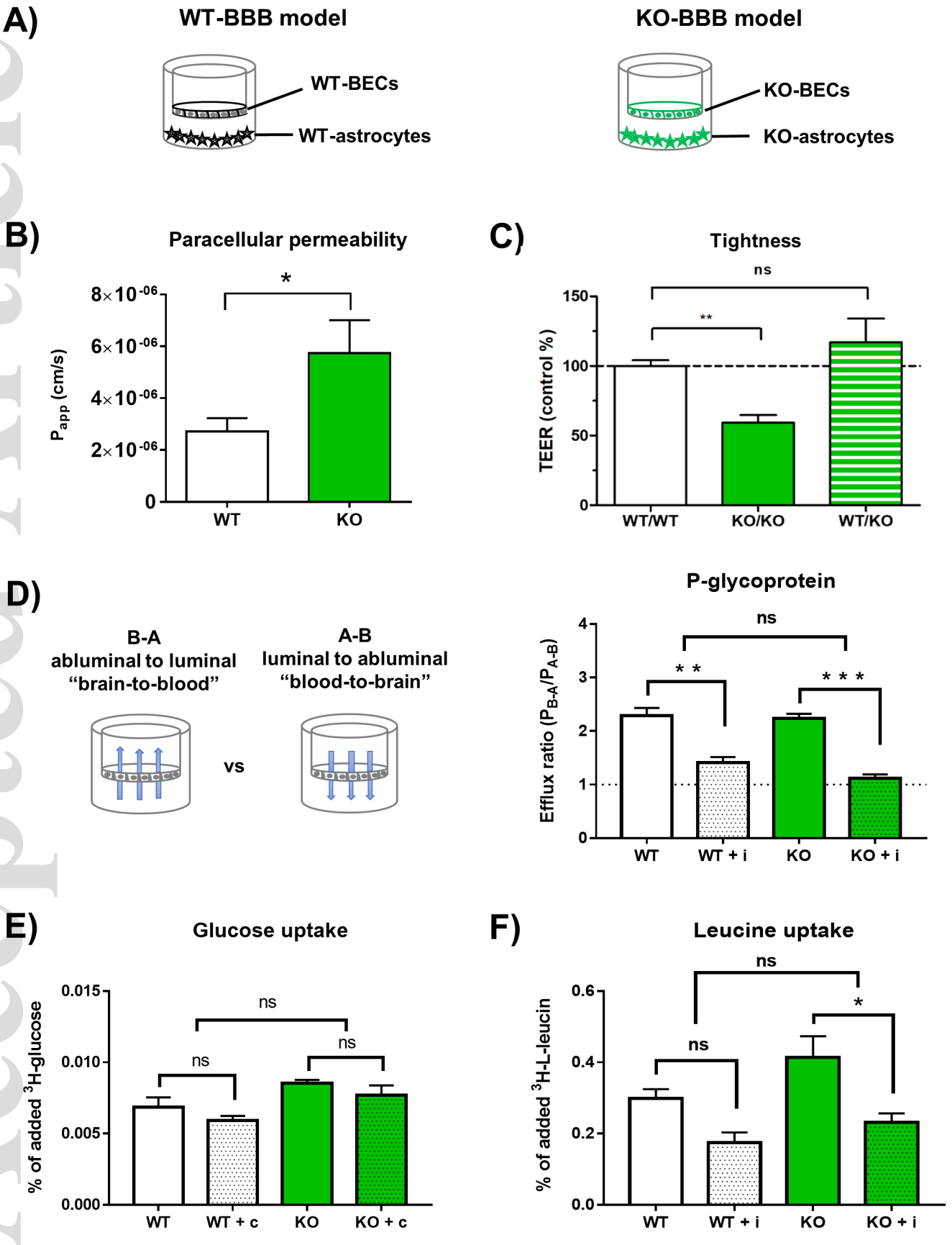

febs_16225_f3.tif

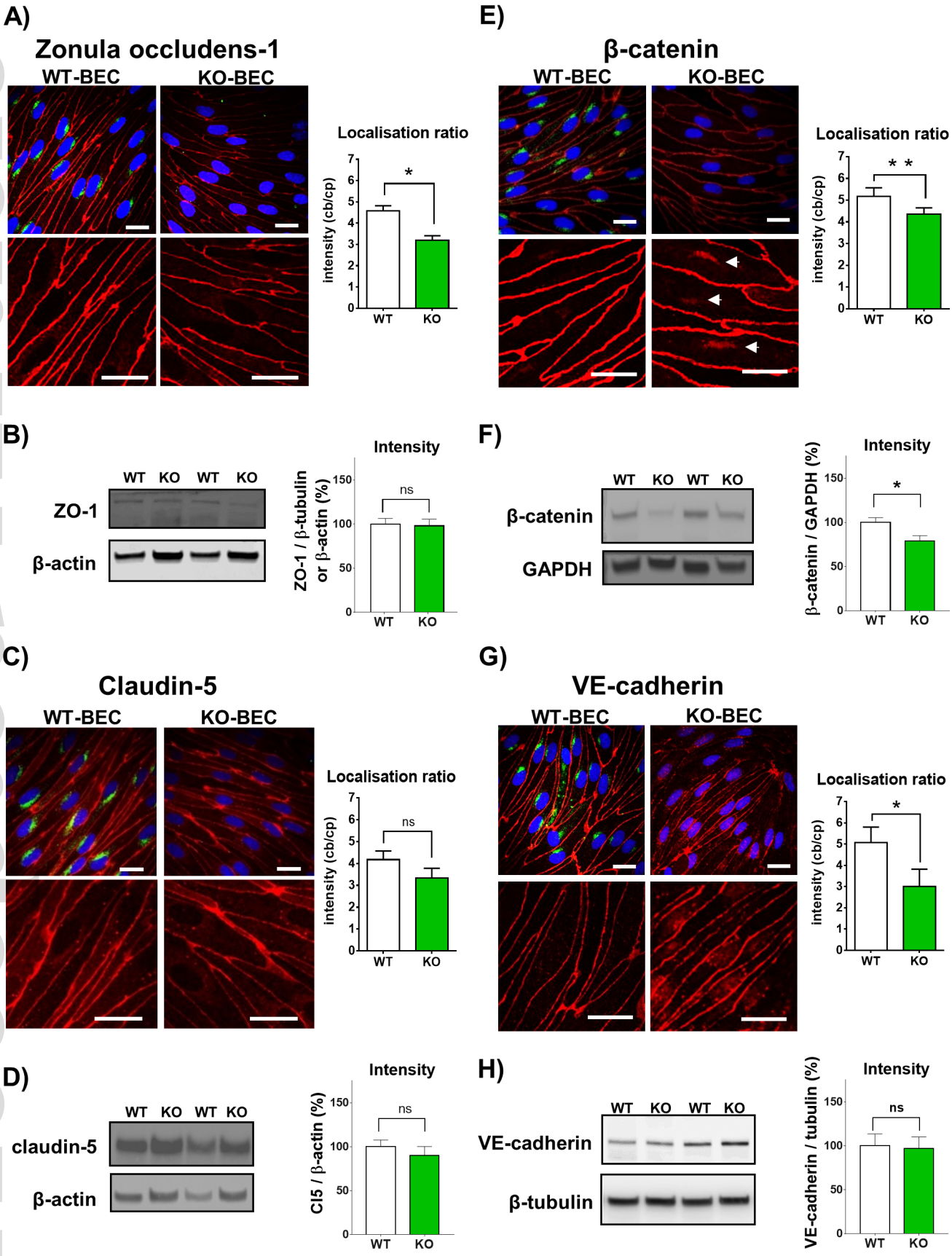

febs_16225_f4.tif

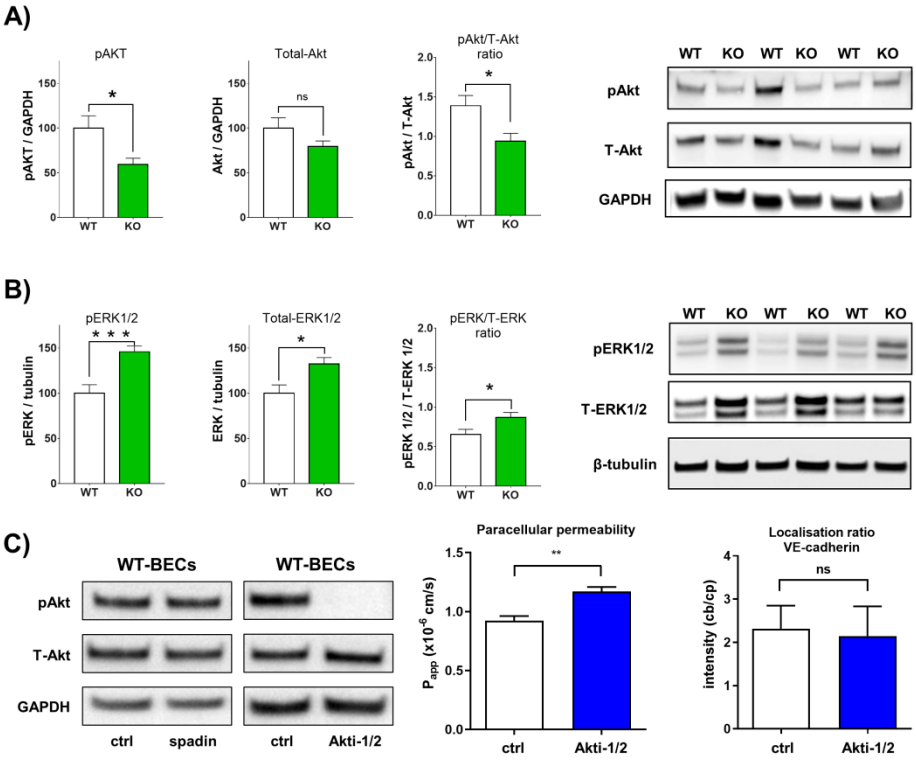

febs_16225_f5.tif